Thai Society of Agricultural Engineering Journal
Volume 21 No. 2 (2015) 50-59
Available online at www.tsae.asia

Research Paper

ISSN 1685-408X

Detection of Chlorotic Cassava Leaves using Image Processing and Discriminant Analysis

Wanrat Abdullakasim[1]*, Kittipong Powbunthorn[1], Jintana Unartngam[2]

[1]Department of Agricultural Engineering, Faculty of Engineering at Kamphaengsaen, Kasetsart University, Nakhon Pathom 73140 Thailand

[2]Department of Plant Pathology, Faculty of Agriculture at Kamphaengsaen, Kasetsart University, Nakhon Pathom 73140 Thailand

*Corresponding author: Tel: +66-34-351-896, Fax: +66-34-351-896, E-mail: fengwra@ku.ac.th

Abstract

Cassava (*Manihot esculenta* Crantz) has been an important industrial crop for Thailand with a tendency of increasing production scale. A profitable cassava production in the future requires not only effective cultivation practices but also an efficient crop protection system, suggesting the necessity of an automated pests and diseases monitoring technology. Modern surveillance operation is usually performed by field imagery and analysis to detect atypical symptoms on the plants. The objective of this study was therefore to assess the feasibility to detect diseased cassava plants in situ by means of conventional image analysis. An image processing technique has been developed for distinguishing healthy and chlorotic leaves which is common symptoms of many cassava diseases. Color images of healthy and diseased cassava leaves were captured in fields with a resolution of 640×480 pixels and overlaid with squared grids of 80×80 pixels. Various color indices including red (*r*), green (*g*), and blue (*b*) chromatic coordinates, contrast indices $r-g$, $g-b$, $(g-b)/|r-g|$ and $2g-r-b$, and hue (*H*), saturation (*S*), and intensity (*I*) were calculated for each grid. The discriminant analysis of principal components method was used to classify the healthy and chlorotic leaves. Total accuracy of the image classification was then evaluated based on Brier score. The results showed that the developed algorithm correctly identified 84.70% of healthy leaves and 79.90% of chlorotic leaves, giving a Brier score of 0.1654. A critical comparison with the neural network classification in an earlier study done by the authors is herein discussed.

Keywords: Cassava, Crop monitoring, Leaf chlorosis, Image processing, Discriminant analysis

1 Introduction

Cassava (*Manihot esculenta* Crantz) has been of important strategic crop for Thailand as it contributes a broad range of industrial applications, largely in agro-industry as well as in bio-energy production. In 2013, cassava plantation area across the country had covered 1.45 million ha, giving a total production of 30.2 million tons with an average yield of 21.8 t ha^{-1} (Office of Agricultural Economics, 2014). In the same year, Thailand exported cassava products for 8.29 million tons, achieving an export value of over 3,190 million USD, ranking first among the world's cassava exporters (Center for Agricultural Information OAE, 2014).

A productive and profitable cassava growing requires an efficient crop protection regime to prevent pests and diseases infestation. Field scouting by human is a common practice to observe the plant health. However, this is laborsome and time consuming even if with an assistance of experienced pathologists particularly in large production scales and when site-specific management is required. An automated crop monitoring system which is capable of providing early detection and tracking of spatial and temporal propagation of pests and diseases has therefore become necessary.

Different types of field surveillance systems have been developed during the past two decades. Schnug et al. (2000) has introduced a Low Altitude Stationary Surveillance Instrumental Equipment (LASSIE), a ground-based remote sensing system which provides dynamic image information so that nutritional status of the crops can be analyzed. Lilienthal et al. (2004)

further emphasized the applicability of the LASSIE system to various agricultural field experimentations. Similarly, Ahamed et al. (2012) developed a tower remote sensing system for monitoring energy crops. A mobile platform has been developed by Hague et al. (2006) using a tractor mounted camera system for crop and weed scanning in widely spaced cereals. Likewise, Xiong et al. (2012) used vehicular platform for sensing bio-energy crops while Zhao et al. (2010) used a mobile robot attached with panchromatic sensor for real-time measurement of the normalized difference vegetation index (NDVI). Aerial imaging is an alternative concept for crop sensing, Xiang and Tian (2011) used an autonomous unmanned aerial vehicle (UAV) for multi-spectral imaging while Samseemuang et al. (2012) developed a helicopter platform for monitoring weed infestation in soybean field. A state-of-the-art review regarding remote sensing method has been reported by Ahamed et al. (2011).

An important routine in such surveillance systems as mentioned above is the analysis process of crop images which is usually developed for a particular purpose. In the diagnosis of pests and diseases, the computer vision has been applied to identify fall armyworm damaged maize plants (Sena et al., 2003), Black Sigatoka infected banana leaves (Camargo and Smith, 2009a), and cotton crops damaged by Southern green stink bug, Bacterial angular, and Ascochyta blight (Camargo and Smith, 2009b). Wang et al. (2008) introduced a segmentation method for diseased leaf images. Many researchers adopted image analysis technique in plant disease scoring (Bock et al., 2008; Wijekoon et al., 2008; Bock et al., 2009; Yang, 2010). Application of machine vision on cassava diseases is, however, relatively few. Aduwo et al. (2010) developed an image analysis technique to classify cassava leaves infected by the mosaic disease (CMD). Abdullakasim et al. (2014) proposed an image processing algorithm for quantifying the severity of cassava brown leaf spot disease.

Most of cassava diseases express symptoms on leaves either in forms of discoloration or distortion. As explained by Calvert and Thresh (2002) for viral diseases, the cassava mosaic disease (CMD) develop either green or yellow patchy mosaic on leaves, whereas the cassava vein mosaic disease (CVMD) express vein chlorosis in chevron pattern or ringspots, and the cassava brown streak disease (CBSD) causes feathery chlorosis along the secondary and tertiary veins. For bacterial and fungal diseases, Hillocks and Wydra (2002) described that cassava bacterial blight disease (CBB) shows water-soaked, angular leaf spot, and leaf blight, while symptoms of the white leaf spot disease (WLS) are circular chlorotic area on the lamina with circular white lesions in the center. Further, diffuse leaf spot disease (DLS) creates large brown spot on the upper side of a leaf but the underside appears grayish. The ring leaf spot disease (RLS) expresses large circular brown spots on both sides of the lamina near the edge of the leaf lobe. The brown leaf spot (BLS) disease is another foliar disease widespreadly found in cassava plantation. The symptoms appear as small brown spot within a darker border on the upper leaf surface and a grayish cast on the lower surface (Teri et al., 1978).

Abdullakasim et al. (2011) has attempted to identify the BLS-infected cassava plants from digital images using different color indices associated with a neural network classification. The best achievable accuracy in image classification was 75.73% for diseased plants and 89.92% for healthy plants.

The objective of this study was to develop an off-line image processing technique which is capable of distinguishing healthy and chlorotic leaves on the diseased cassava plants in natural field conditions, by extending the analysis of color parameters used by Abdullakasim et al. (2011) and re-classify using discriminant analysis method.

2 Materials and Method

2.1 Experimental site and plant materials

The cassava plants were grown at an experimental field of Kasetsart University, Kamphaeng Saen Campus, Nakhon Pathom, Thailand ($14^{\circ}2'11''$N, $99^{\circ}57'56''$E). Important soil properties at the site are given in Table 1. The cassava cultivar was *Rayong 5* which has been classified as medium-resistant cultivar in terms of brown leaf spot disease resistance (Kampanich, 2003), but highly susceptible to bacterial blight disease (Srisura and Lertsuchatavanich, 2014). The plant age at experimentation was six months, at which stage their

canopy had fully developed. The chlorotic leaves caused by brown leaf spot disease were found scattering on some plants across the field, but no inoculation treatment was taken place in this study.

Table 1 Soil properties at cassava growing site

Property	Value
Texture	Clay loam
pH	7.6
EC_a (dS/m)	0.409
Organic matter (%)	1.82
Phosphorus (mg kg^{-1})	48
Potassium (mg kg^{-1})	60

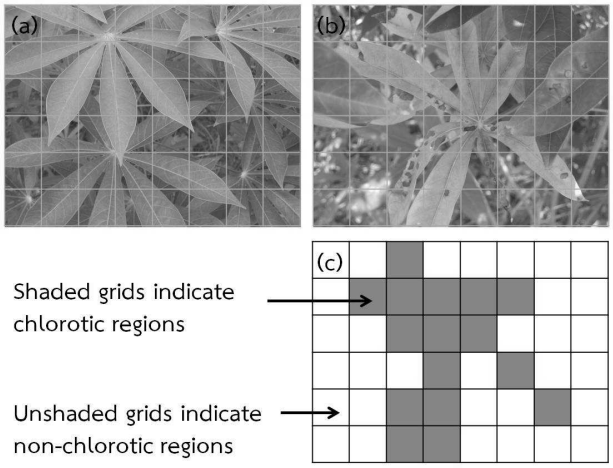

Figure 1 Sample images of: (a) healthy leaves, (b) chlorotic leaves, and (c) chlorotic regions mapping.

2.2 Image acquisition and processing

Color images of both healthy and chlorotic cassava leaves were captured manually at several random positions approximately 1.0 m above the plants using a digital camera (Canon, IXY55, Japan). The camera was set to operate in automatic mode with a resolution of 640×480 pixels under natural sunlight at solar noon. Illuminance at the leaf positions measured by a light meter ranged from 412,000 to 680,000 lux. The image dataset consisted of 80 images of healthy leaves, and another 80 images for chlorotic leaves.

The image was pre-processed and analyzed by programming particular routines using Image Processing Toolbox™ on MATLAB® platform. The original image was automatically overlaid with 48 grids arranging in 6 rows and 8 columns, inside which contained 80×80 pixels each. The image that contained chlorotic leaves when devided into grids, however, appeared in both non-chlorotic (e.g. healthy leaves, stems, ground, etc.) and true chlorotic regions (Figure 1). Each grid was designated either as healthy, or chlorotic region if appeared the discolored area larger than 50%. Counting of these grids yielded a total number of 5,270 grids for healthy, and 2,410 grids for chlorotic leaves. The primary red (*R*), green (*G*), and blue (*B*) color intensities of each single pixel were read by the program for subsequent transformation to secondary parameters.

Various color parameters introduced by Woebbecke et al. (1995) were used in this study. These included chromatic coordinates (*r*, *g*, and *b*) which are defined as:

$$r = \frac{R^*}{R^* + G^* + B^*},$$

$$g = \frac{G^*}{R^* + G^* + B^*},$$

$$b = \frac{B^*}{R^* + G^* + B^*}, \qquad (1)$$

where

$$R^* = \frac{R}{R_m}, \quad G^* = \frac{G}{G_m}, \quad B^* = \frac{B}{B_m} \qquad (2)$$

and R_m, G_m, and B_m = 255, are the maximum tonal value for each primary color.

Another group of color indices including *r*–*g*, *g*–*b*, $(g-b)/\left|r-g\right|$ and 2*g*–*r*–*b* were calculated to magnify the contrast between leaves and plant parts of different color. Preliminary test indicated the possibility of obtaining a zero in the denominator of the index $g-b)/\left|r-g\right|$, denominator values between –0.01 and +0.01 were therefore rounded up to 0.01.

The hue, saturation, and intensity (HSI) color space was also used in addition to the chromatic coordinates. Modifed hue (*H*), saturation (*S*) and intensity (*I*) were derived from *R, G, and B* values as follows (Gonzalez and Woods, 2010):

$$H = \begin{cases} \theta & \text{if } B \le G \\ 360 - \theta & \text{if } B > G \end{cases} \quad (3)$$

where

$$\theta = \cos^{-1}\left\{ \frac{\frac{1}{2}\left[(R-G)+(R-B)\right]}{\left[(R-G)^2+(R-B)(G-B)\right]^{1/2}} \right\}, \quad (4)$$

$$S = 1 - \frac{3}{(R+G+B)}\left[\min(R,G,B)\right], \quad (5)$$

and

$$I = \frac{1}{3}\left(R+G+B\right) \quad (6)$$

Mean value of each color index was calculated across the total 6,400 pixels (80×80) for each grid and used as a representive value in the classification.

2.3 Image classification using discriminant analysis

The discriminant analysis method was used to classify the images of healthy and chlorotic cassava leaves. The image dataset was divided into two sets i.e. calibration and validation. From the total 5,270 grids of healthy leaves, 3,247 (61.6%) of which were randomly selected for developing the discriminant functions and the rest were used for validation. Similarly, 1,553 (64.4%) out of 2,410 samples of chlorotic leaves were used for calibration and the remainders were used for validation.

Dependency among color indices were examined by multicollinearity test using Pearson's product moment correlation coefficeint (r_{xy}), associated with the collinearity statistics; tolerance (*T*), and variance inflation factor (*VIF*) which can be determined by equations (7), (8) and (9) respectively.

$$r_{xy} = \frac{n\sum x_i y_i - \sum x_i \sum y_i}{\sqrt{\left(n\sum x_i^2 - \left(\sum x_i\right)^2\right)\left(n\sum y_i^2 - \left(\sum y_i\right)^2\right)}} \quad (7)$$

where x_i and y_i represents the two color parameters to be tested, and n is the number of data pairs.

$$T = 1 - R_i^2 \quad (8)$$

and

$$VIF = \frac{1}{1-R_i^2} \quad (9)$$

where R_i^2 is the coefficient of determination for each pair of color indices.

In image classification, feature descriptors should be independent against each other since dependency among them may results in misleading interpretation which in turn affecting the accuracy of classification. However, if significant multicollinearity was found, subsequent procedures to group those correlated parameters should be applied. In this study, factor analysis method as described by Landau and Everitt (2004) was used to rearrange similar color indices into new orthogonal components. The SPSS software (SPSS Inc.) was used to implement these analyses. The number of factors to be extracted was determined by Kaiser stopping criterion i.e. all factors with eigenvalues greater than 1.0 would be adopted. Varimax rotation method was selected to obtain orthogonal solution. The rotated solution would describe factor loadings for each individual color parameter in the dataset. Discriminant functions for image classification were then derived based on these independent principal components (Landau and Everitt, 2004).

In order to evaluate overall performance of image classification and to further compare the results with other classification methods, the Brier score (*BR*) was calculated according to equation (10):

$$BR = \frac{1}{N}\sum_{i=1}^{N}(f_t - o_t)^2 \quad (10)$$

where N is the number of predicting instances, f_t is the probability that was predicted, o_t is the actual outcome of the prediction at instance t, representing by 0 if the prediction was not correct, and 1 if the prediction was correct. Brier score is unitless and ranges from 0 to 1. The smaller the score is, the better is the ability to classify the image.

3 Results and Discussion

3.1 General characteristics of color indices

The color parameters of healthy and chlorotic cassava leaves have been obtained from processed images. Ranges of each parameter were observed to ensure the generality of the data. As shown in Table 2, the *r* and *g* coordinates ranged widely from closed to their theoretical minimum, zero, to their maximum, one, while the range of *b* was slightly narrower by nature of leaf color. Likewise, comprehensive ranges were found for *S* and *I* values, indicating varying levels of color purity and light intensity in the images. The *H* value fell into a limited range of approximately 0.1 to 0.4, corresponding to the hue angles of 36 and 144° which are the sectors of yellow and green colors respectively.

Table 2 Ranges of color indices.

Index	Range of index value	
	Healthy	Chlorotic
r	0.1044–0.7790	0.1325–0.9184
g	0.1419–0.9359	0.1808–0.9771
b	0.0617–0.7358	0.0261–0.6790
r–g	–0.3036–0.0539	–0.2793–0.0842
g–b	0.0282–0.4880	0.0409–0.5425
$(g-b)/\lvert r-g \rvert$	0.1579–10.5600	0.5315–26.7671
2g–r–b	0.0187–0.7548	0.0548–0.7469
H	0.1049–0.4382	0.1117–0.3993
S	0.0673–0.8432	0.1081–0.9439
I	0.1168–0.7882	0.1168–0.8370

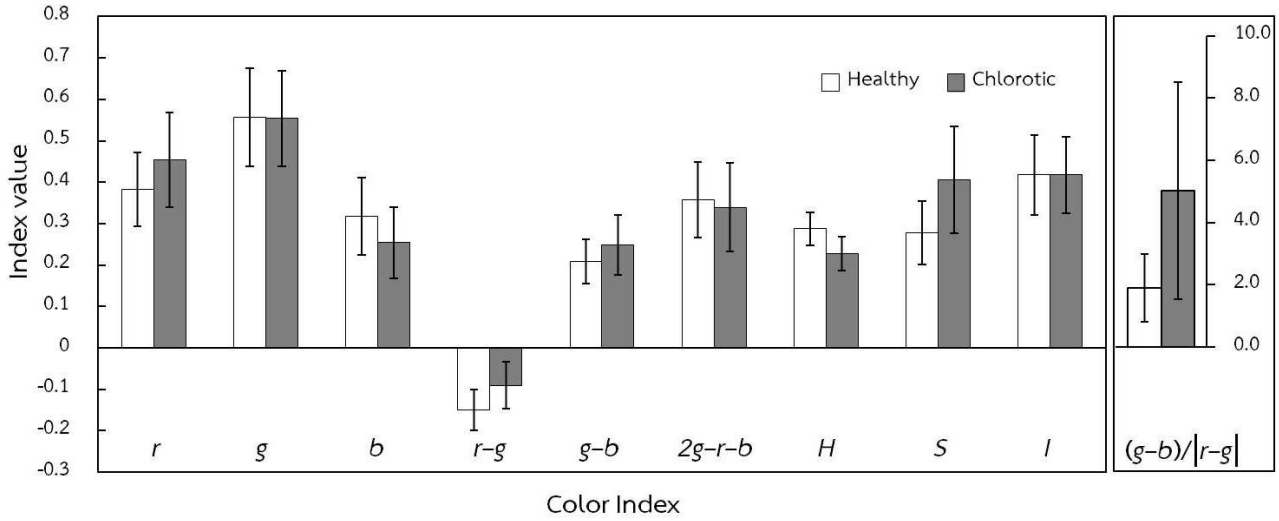

Figure 2 Comparison between index values of healthy and chlorotic leaves. Error bars indicate standard deviations of the means.

Mean values of each color index for the healthy and chlorotic leaves have been compared (Figure 2). The chromatic *r* of the diseased leaves was greater than that of the healthy leaves, obviously describing the redness of chlorotic leaves. The *b* coordinate resulted in the opposite while the *g* index was more or less not different. The mean *H* value of the diseased leaves was 0.2275 (81.9°), corresponding to the yellowish sector, while the mean *H* for healthy leaves was 0.2874 (103.5°) i.e. falling into the green sector. The *H* index is therefore a good descriptor in differentiating the diseased plants from the healthy plants. The *S* index was appreciably greater in chlorotic leaves while the achromatic *I* were not different and hence may not be a good parameter. The *r–g* index of both healthy and chlorotic leaves always resulted in negative values while the *g–b* and *2g–r–b* were positive. These secondary indices, however, did not provide clear discrimination between the healthy and diseased leaves. Better contrast between the healthy and chlorotic leaves was achieved from the ratio index $(g-b)/\lvert r-g \rvert$, although with increased standard deviation. This result is similar to the findings of Woebbecke et al. (1995) even though in their study

this particular index was used to distinguish between weeds and soil. The present result thus suggested that the ratio index was still applicable for healthy and diseased leaves discrimination although in which case the contrast in color may be smaller than that between the weeds and soil.

3.2 Multicollinearity of color parameters and factor analysis

Pearson's product moment correlation tests showed significant dependency for all color indices. This was not beyond expectation because all color indices were actually derived from the same primary *R, G and B*. The results of tolerance, *T* and *VIF* analysis also supported this fact (Table 3). Except *g–b*, the T values for all color indices approached zero and the *VIF* values were relatively high, implying that all color indices, excluding the *g–b*, had linear inter-correlations among them. Of these, *H* and $(g-b)/|r-g|$ seems to be of best parameters after *g–b* in terms of independency.

Factor analysis has been performed to reduce color indices by creating new factors, i.e. principal components (PCs) that are mutually orthogonal. In Table 4, the software initially generated ten new factors, however, considering from eigenvalues of greater than 1.0 resulted in that only the first three components A component transformation matrix has been generated, providing coefficients for deriving transformation equations of each principal component as expressed by eq. (11)–(13). were remained. With these three PCs, over 95% of variance could be covered. As a consequence, the original color indices were rearranged either into PC1, PC2 or PC3 depending on loading values. Table 5 shows the rorated component matrix describing the membership of each color index. The PC1 consisted of five parameters; *b*, *I*, *g–b*, *g* and *S*. PC2 included four parameters; *r–g*, *H*, $(g-b)/|r-g|$ and *r*, while only *2g–r–b* constituted PC3. Figure 3 graphically represents the distribution of color indices with respect to the three principal components.

Table 3 Results of collinearity test by *T* and *VIF* statistics.

Color index	*T*	*VIF*
r	0.021	46.799
g	0.029	34.314
b	0.027	37.317
r–g	0.010	97.523
g–b	-	-
$(g-b)/\|r-g\|$	0.236	4.233
2g–r–b	0.012	85.969
H	0.129	7.754
S	0.065	15.449
I	0.078	12.891

Table 4 Total variance explained by principal component analysis.

Component	Initial eigenvalue			Rotation sums of squared loadings		
	Total	% of variance	Cumulative %	Total	% of Variance	Cumulative %
1	3.963	39.634	39.634	3.963	39.634	39.634
2	3.316	33.159	72.793	3.316	33.159	72.793
3	2.247	22.465	95.258	2.247	22.465	95.258
4	.264	2.636	97.894	-	-	-
5	0.092	0.924	98.819	-	-	-
6	0.056	0.557	99.376	-	-	-
7	0.035	0.346	99.722	-	-	-
8	0.018	0.175	99.898	-	-	-
9	0.010	0.102	100.000	-	-	-
10	0.000	0.000	100.000	-	-	-

$$PC1 = 0.157r + 0.177g + 0.245b + 0.043(r-g) - 0.183(g-b) - 0.058\frac{(g-b)}{|r-g|} - 0.144(2g-r-b) + 0.073H - 0.166S + 0.210I \quad (11)$$

$$PC2 = 0.192r + 0.027g - 0.054b + 0.269(r-g) + 0.032(g-b) + 0.263\frac{(g-b)}{|r-g|} - 0.141(2g-r-b) - 0.266H + 0.154S + 0.060I \quad (12)$$

$$PC3 = 0.194r + 0.310g + 0.040b - 0.174(r-g) + 0.299(g-b) + 0.026\frac{(g-b)}{|r-g|} + 0.298(2g-r-b) + 0.070H + 0.226S + 0.211I \quad (13)$$

Table 5 Rotated component matrix.

Color index	PC1	PC2	PC3
b	0.969	–	–
I	0.834	0.200	0.473
g–b	–0.725	–	0.672
g	0.700	–	0.696
S	–0.658	0.512	0.508
r–g	–	0.892	–0.391
H	0.290	–0.882	–
$(g-b)/\lvert r-g \rvert$	–0.231	0.872	–
r	0.621	0.638	0.436
2g–r–b	–0.571	–0.468	0.670

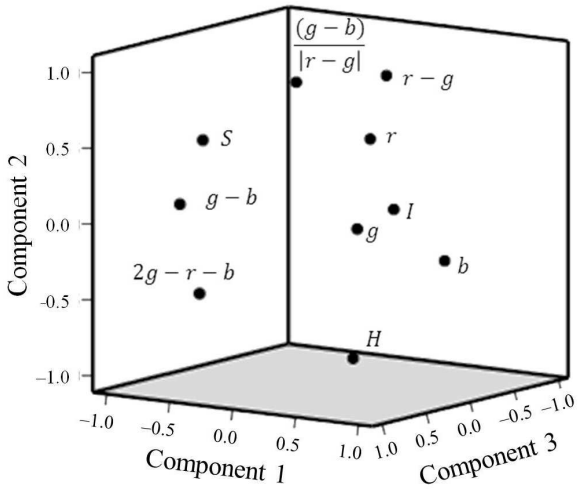

Figure 3 Distribution of color indices in space of principal components.

3.3 Image classification by discriminant analysis

Discriminant functions for differentiating the groups of healthy and chlorotic leaves have been developed as functions of PC1, PC2 and PC3 using the calibration dataset, expressed by eq. (14) and (15):

$$HG = 0.317(PC1) - 0.780(PC2) - 1.155(PC3) - 0.901, \quad (14)$$

and

$$CG = -0.451(PC1) + 1.488(PC2) + 0.380(PC3) - 1.409. \quad (15)$$

For each image, substituing PC1, PC2 and PC3 values in both equations returned the scores for healthy (HG) and the chlorotic (CG) groups. A particular image was classified into the group that possessed the greater score. Applying the discriminant fundtions across the entire image dataset resulted in the distribution of discriminant scores shown in Figure 4.

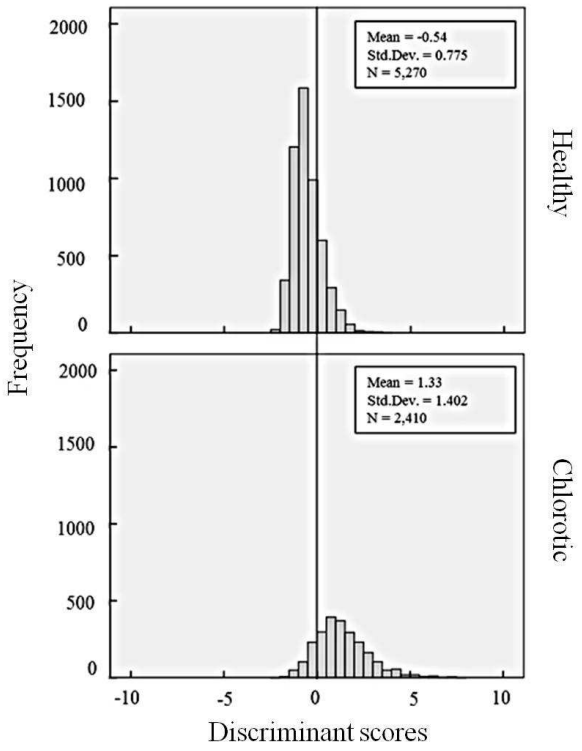

Figure 4 Distribution of discriminant scores for healthy and chlorotic groups.

The histogram revealed some overlapping between the healthy and chlorotic groups, however, a significant mean difference was observed, demonstrating that the majority of images were successfully classified. In other

words, the discriminant functions were sufficiently potential to discriminate the healthy and the diseased plants.

The accuracy of image classification has been evaluated (Table 6). For the calibration dataset itseft, the discriminant analysis was able to classify 89.0% of healthy leaves and 72.6% of chlorotic leaves. Further testing using the validation dataset resulted in that 84.7% of healthy leaves and 79.9% of chlorotic leaves images were correctly recognized. Calculation of Brier score yielded a value of 0.1654.

In our previous study (Abdullakasim et al., 2011) which relied on neural network classification, the highest successful classification rate was 75.73% for diseased leaves and 89.92% for healthy leaves, giving a Brier score of 0.1431. The present study therefore provided better recognition of diseased leaves but poorer identification of healthy leaves. The overall performance decided by Brier score indicated that the discriminant analysis could be an alternative approach, however, did not provide an improved result.

Table 6 Accuracy of image classification.

Dataset	Actual group	Total number of image	Group as classified by discriminant analysis	
			Healthy	Chlorotic
Calibration	Healthy	3,247	2,889 (89.0%)	358 (11.0%)
	Chlorotic	1,553	426 (27.4%)	1,127 (72.6%)
Validation	Healthy	2,023	1,714 (84.7%)	309 (15.3%)
	Chlorotic	857	172 (20.1%)	685 (79.9%)

The present study suggested a feasibility to detect chlorotic leaves on diseased cassava plants in field condition by means of computer vision. The results, however, indicated some possibility of misclassification of the diseased plants. This may be attributed to many reasons. First, the leaves images have been analyzed without segmentation to standout the leaf features from its background (e.g. stems, soil, weeds, residues, etc.). Remaining of irrelevant objects could therefore mislead color interpretation by the classification algorithm. Second, misidentification of the diseased plants is likely to have been occurred due to the variation in illuminating condition in the fields. Regarding which, it also depends on the position of camera with respect to the cassava canopy and shading caused by leaves overlapping and inclination. Third, the size of grids overlaid on the image has influenced the designation of gird type when both the healthy and chlorotic pixels presented in the same grid. In order to improve the detection accuracy, more elaborate experimentation and analysis algorithm must be designed.

4 Conclusions

An image processing technique based on different color indices has been developed for detection of clorotics leaves on the cassava plants in field condition. The best identification accuracy was 84.7% of healthy plants and 79.9% of diseased plants. Discriminant analysis approach provided better understanding about characteristics of the color descriptors comparing to the neural network although its total performance was more or less the same. To some extent, this study suggested a feasibility to detect suspicious symtoms of some foliar diseases infecting cassava plants from conventional image analysis. These findings can be of fundamentals for further development a field scouting system. Futher improvement of the technique might be done by accounting the effect of lighting condition, camera position, and size of grid in mapping, associated with proper image segmentation. Selection of appropriate image features should also be considered.

5 Acknowledgement

The present research work has been financially supported by Kasetsart University Research and Development Institute (KURDI).

6 References

Abdullakasim, W., Powbunthorn, K., Unartngam, J., Takigawa, T. 2011. An images analysis technique for recognition of brown leaf spot disease in cassava. Journal of Agricultural Machinery Science 7(2), 165–169.

Abdullakasim, W., Powbunthorn, K., Unartngam, J. 2014. Quantification of the severity of brown leaf spot disease in cassava using image analysis. Thai Society of Agricultural Engineering Journal 20(2), 24–32.

Aduwo, J.R., Mwebaze, E., Quinn, J.A. 2010. Automated vision-based diagnosis of cassava mosaic disease.

Workshop on Data Mining in Agriculture (DMA 2010), Berlin.

Ahamed, T., Tian, L., Jian, Y., Zhao, B., Liu, H., Ting, K.C. 2012. Tower remote sensing system for monitoring energy crops; image acquisition and geometric corrections. Biosystems Engineering 112(2), 93–107.

Ahamed, T., Tian, L., Zhang, Y., Ting, K.C. 2011. A review of remote sensing methods for biomass feedstock production. Biomass & Bioenergy 35(7), 2455–2469.

Bock, C.H., Parker, P.E., Cook, A.Z., Gottwald, T.R. 2008. Visual rating and the use of image analysis for assessing different symptoms of citrus canker on grapefruit leaves. Plant Disease 92(4), 530–541.

Bock, C.H., Cook, A.Z., Parker, P.E., Gottwald, T.R. 2009. Automated image analysis of the severity of foliar citrus canker symptoms. Plant Disease 93(6), 660–665.

Calvert, L.A., Thresh, J.M. 2002. The Viruses and Virus Diseases of Cassava. *In*: Hillocks, R. J., Thresh, J. M., Bellotti, A.C. (Eds), Cassava: Biology, Production and Utilization. CAB International, UK.

Camargo, A., Smith, J.S. 2009a. An image-processing based algorithm to automatically indentify plant disease visual symptoms. Biosystems Engineering 102, 9–21.

Camargo, A., Smith, J.S. 2009b. Image pattern classification for the identification of disease causing agents in plants. Computers and Electronics in Agriculture 66, 121–125.

Center for Agricultural Information OAE. 2014. Thailand Foreign Agricultural Trade Statistics 2012. Office of Agricultural Economics, Ministry of Agriculture and Cooperatives, Bangkok, Thailand.

Gonzalez, R.C., Woods, R.E. 2010. Digital Image Processing. Pearson Education, Inc., USA.

Hague, T., Tillett, N. D., Wheeler, H. 2006. Automated crop and weed monitoring in widely spaced cereals. Precision Agriculture 7, 21–32.

Hillocks, R.J., Wydra, K. 2002. Bacterial, fungal and nematode disease. *In*: Hillocks, R. J., Thresh, J. M., Bellotti, A.C. (Eds), Cassava: Biology, Production and Utilization. CAB International, UK.

Kampanich, W. 2003. Investigation on Screening Methods for Cassava Resistant Varieties to Brown Leaf Spot Disease (*Cercospora henningsii* Allescher)**.** Master's dissertation, Kasetsart University, Thailand (in Thai).

Landau, S., Everitt, B. S. 2004. A Handbook of Statistical Analyses using SPSS. Chapman and Hall/CRC Press LLC, USA.

Lilienthal, H., Ponomarev, M., Schnug, E. 2004. Application of LASSIE to improve agricultural field experimentation. Landbauforschung Volkenrode 54, 21–26.

Office of Agricultural Economics. 2014. Agricultural Statistics of Thailand 2012. Ministry of Agriculture and Cooperatives, Bangkok, Thailand.

Samseemoung, G., Soni, P., Jayasuriya H.P.W., Salokhe, V.M. 2012. Application of low altitude remote sensing (LARS) platform for monitoring crop growth and weed infestation in a soybean plantation. Precision Agriculture 13, 611–627.

Schnug, E., Haneklaus, S., Lilienthal, H., Panten, K. 2000. LASSIE—an innovative approach for the continuous remote sensing of crops. Aspects of Applied Biology 60, 147–153.

Sena Jr. D.G., Pinto, F.A.C., Queiroz, D.M. Viana, P.A. 2003. Fall Armyworm Damaged Maize Plant Identification using Digital Images. Biosystems Engineering 85, 449–454.

Srisura, C., Lertsuchatavanich, U. 2014. Pathogenicity disease virulence tests of *Xanthomonas axonopodis* pv. *manihotis* on cassava Huaybong 80 and Rayong 5 cultivars in greenhouse. Proceedings of the 52nd Kasetsart University Annual Conference, 4–7 February 2014, Bangkok, 489–496 (in Thai with English abstract).

Teri, J.M., Thurston, H.D., Lozano, J.C. 1978. The Cercospora leaf diseases of cassava. Proceedings Cassava Protection Workshop, CIAT, Cali, Colombia 7–12 November 1977, 101–116.

Wang, L., Yang, T., Tian, Y. 2008. Crop disease leaf image segmentation method based on color features. In: Daoliang, L. (Eds.), Computer and Computing Technologies in Agriculture, Vol.1. Springer, Boston. pp. 713–717.

Wijekoon, C.P., Goodwin, P.H., Hsiang, T. 2008. Quantifying fungal infection of plant leaves by digital image analysis using Scion Image software. Journal of Microbiological Methods 74, 94–101.

Woebbecke, D.M., Meyer, G.E., Von Bargen, K., Mortensen, D.A. 1995. Color indices for weed identification under various soil, residue, and lighting conditions. Transactions of the ASAE 38(1), 259–269.

Xiang, H., Tian, L. 2011. Development of a low-cost agricultural remote sensing system based on an autonomous unmanned aerial vehicle (UAV). Biosystems Engineering 108(2), 174–190.

Xiong, Y., Tian, L., Ahamed, T., Zhao, B. 2012. Development of the reconfigurable data acquisition vehicle for bio-energy crop sensing and management. Journal of Mechanical Design, 134(1), 015001.

Yang, C.-M. 2010. Assessment of the severity of bacterial leaf blight in rice using canopy hyperspectral reflectance. Precision Agriculture 11(1), 61–81.

Zhao, B., Tian, L., Ahamed, T. 2010. Real time NDVI measurement using low cost panchromatic sensor for mobile robot. Environment Control in Biology, 48(2), 73–79.